CrystEngComm

PAPER

View Article Online
View Journal | View Issue

Published on 15 July 2014. Downloaded by Indian Institute of Technology Kharagpur on 18/12/2014 03:50:17.

Cite this: *CrystEngComm*, 2014, **16**, 8546

Room temperature light-induced recrystallization of Cu_2O cubes to CuO nanostructures in water†

Yulyi Na,[a] Sung Woo Lee,[b] Nitish Roy,[c] Debabrata Pradhan*[c] and Youngku Sohn*[a]

Received 9th June 2014,
Accepted 11th July 2014

DOI: 10.1039/c4ce01174k

www.rsc.org/crystengcomm

The mechanism of temperature-assisted Cu and Cu_2O oxidation in oxygen and subsequent CuO nanowire growth is well known. Here, we report a simple light-induced process for the recrystallization of Cu_2O cubes to [010] growth-directed CuO nanoribbons in water at room temperature. This was attributed to the formation and participation of $^{\bullet}OH$ and $^{\bullet}O_2^-$ active species in water as well as the outward diffusion of Cu ions leading to the formation of CuO nanoribbons along unstable {010} facets on the surface of Cu_2O cubes. The oxidation was significantly suppressed under dark conditions or by active species scavengers, confirming the strong role of visible light. CO oxidation activity of nanoribbons was found to be superior to that of cubes. Our unique light-induced recrystallization of Cu_2O to CuO in water provides new insight and better understanding of the oxidation mechanism of Cu_2O, enabling tailoring of nanostructures by varying types of light (sun, incandescent and fluorescent) and opening a new strategy for development of energy- and environment-related Cu oxide nanomaterials.

1. Introduction

The abundance of copper and Cu oxides (Cu_2O and CuO) in nature and their cost-effective applications related to energy, the environment, and sensors have led researchers to investigate their fundamental nature and to develop various nanostructures (*e.g.*, cubes, octahedrons, dodecahedrons, plates, wires and hollows) from these compounds.[1–31] The effects of morphology, crystallinity and relative surface reactivity during interfacial heterogeneous liquid–solid (and gas–solid) chemical reactions have been actively examined for Cu oxide materials.[6–9] Hua *et al.*[7] and Park *et al.*[8] reported a change in the morphology and oxidation state of Cu_2O cubes to a belt-shaped and hollow structure, respectively, in response to reactions in ammonia solution. Chen and Xue synthesized Cu oxide materials with various shapes by a chemical transformation method.[22–25] Several studies have reported the synthesis of CuO nanowires (or nanoribbons) at room temperature using a wet-chemical method or a mechanochemical method.[22–25] In these studies, $Cu(OH)_2$ was initially formed and decomposed to CuO in a reaction in which the OH^-/Cu^{2+} ratio plays an important role in the formation of nanoribbons.[23,24] CuO materials have also been prepared *via* an oxidation route (Cu → Cu_2O → CuO) in the gas phase at high temperature.[32–39] When Cu plates are heated at high temperature under an O_2 atmosphere, Cu_2O is initially formed on the surface, after which less symmetric CuO is generated. Song *et al.* introduced a microfluidic reactor process to synthesize Cu nanoparticles with a smaller and narrower size distribution.[40,41] Among many applications, catalytic activities of Cu oxides have been attracting a great deal of interest with respect to environmental and energy issues,[42–51] which include CO oxidation,[48–55] dye degradation,[4,42–44] and water splitting.[45–47] For example, Huang *et al.* prepared diversely shaped Cu_2O nanocrystals by varying the amount of $NH_2OH{\cdot}HCl$ and reported that rhombic dodecahedra with only {110} exposed facets showed the best photocatalytic activity for methyl orange (MO) degradation owing to the high density of surface Cu atoms.[4] Leng *et al.* synthesized polyhedral 50-facet Cu_2O microcrystals and found enhanced CO oxidation activity relative to those of rhombic dodecahedral, octahedral and cubic Cu_2O crystals.[51]

Understanding the oxidation mechanism of Cu and Cu_2O to CuO as well as the reduction of CuO is technologically and fundamentally important.[2,32–39] Recent studies have focused on the driving force and growth mechanism of CuO nanowires during the thermal oxidation of Cu metals in the gas phase.[32–39] However, oxidation of Cu_2O to CuO in the liquid phase (in water) has not yet been reported. Here, we report the light-induced oxidation of Cu_2O to CuO in water. Specifically, we present the change in morphology, crystallinity, oxidation states and liquid–solid heterogeneous Cu_2O oxidation

[a] *Department of Chemistry, Yeungnam University, Gyeongsan 712-749, Republic of Korea. E-mail: youngkusohn@ynu.ac.kr*
[b] *Center for Research Facilities, Chungnam National University, Daejeon 305-764, Republic of Korea*
[c] *Materials Science Centre, Indian Institute of Technology, Kharagpur 721 302, W. B., India. E-mail: deb@matsc.iitkgp.ernet.in*

† Electronic supplementary information (ESI) available. See DOI: 10.1039/c4ce01174k

This journal is © The Royal Society of Chemistry 2014

Published on 15 July 2014. Downloaded by Indian Institute of Technology Kharagpur on 18/12/2014 03:50:17.

reactions induced by visible light in water at room temperature. This study also provides a new facial strategy for synthesis of CuO nanoribbons (or nanowires).

2. Experimental section

Materials and synthesis

Cu_2O cubes were prepared by a precipitation method. Briefly, 5.0 mL of 0.1 M $CuCl_2$ (Daejung Chem., 99.0%) was mixed with 3.0 mL of 0.1 M NaOH solution and stirred. Next, 5.0 mL of 0.1 M ascorbic acid solution was added, after which the solution was stirred for 30 min. Upon completion of the reaction, we centrifuged the precipitates, thoroughly washed them with water (or ethanol), and then dried the samples in an oven at 80 °C for further characterization.

Characterization

To examine the change in morphology and crystal structure of Cu_2O cubes, we stored the Cu_2O cubes separately in water (in the presence of sun, fluorescent, and incandescent light), ethanol (light), and water (dark). The surface morphology was then examined by scanning electron microscopy (SEM, Hitachi SE-4800). Transmission electron microscopy (TEM) study was carried out using a FEI Tecnai G^2 TEM at an operating voltage of 200 kV. X-ray diffraction (XRD) patterns were observed with a PANalytical X'Pert Pro MPD diffractometer operated at 40 kV and 30 mA using Cu Kα radiation. UV-vis absorption spectra of powder samples were obtained using a Varian Cary 5000 UV-vis-NIR spectrophotometer. The BET surface area was measured using a Quantachrome ChemBET TPR/TPD analyzer.

Oxidation mechanism tests

An indirect scavenger method was used to examine the roles of e^-, $^{\bullet}OH$ and $^{\bullet}O_2^-$ species in Cu_2O oxidation. We added Ag^+, isopropyl alcohol (IPA) and benzoquinone (BQ) as scavengers for e^-, $^{\bullet}OH$ and $^{\bullet}O_2^-$, respectively, into Cu_2O-dispersed water solution under visible light irradiation. After visible light irradiation for the specified duration, we collected the Cu_2O cubes and measured their XRD patterns. The role of species active in the Cu_2O oxidation was tested by the photocatalytic dye degradation of methyl orange (MO, 10 ppm = mg L^{-1}) under visible light irradiation (halogen lamp) using a UV-visible absorption spectrometer (Jasco V-530).

Catalytic activity tests

MO degradation with Cu_2O cubes was also tested with and without scavengers (IPA and BQ). OH radical formation in the presence of Cu_2O cubes under visible light was tested by photoluminescence using terephthalic acid. A SCINCO FluoroMate FS-2 was used to detect the photoluminescence signal at an excitation wavelength of 315 nm. CO oxidation experiments were performed with 10 mg of catalyst at a heating rate of 20 °C min^{-1} under a mixture of CO (1%) and O_2 (2.5%) in N_2 using an SRS RGA200 quadrupole mass spectrometer.

3. Results and discussion

Fig. 1A (top left) and B (middle left) show the SEM images of the as-prepared samples fully washed with ethanol and water, respectively, upon completion of the synthesis. Both samples were found to consist of cube-shaped particles, but the shape for the water-washed sample appeared to be slightly distorted. Interestingly, the morphology of Cu_2O cubes was changed to nanoribbon-like structures upon storage for longer durations (8, 17 and 22 days) in water in a laboratory environment with light exposure, as shown in the SEM images. After 22 days in water with light exposure (bottom right), the cubes were almost completely changed to nanoribbons (ESI,† Fig. S1). However, the same was not observed for Cu_2O cubes stored in ethanol with light exposure for 22 days (top right) or in water under dark conditions. The XRD patterns in the inset and ESI† (Fig. S2) show that the as-prepared Cu_2O cubes washed with ethanol have a cubic ($Pn\bar{3}m$, JCPDS 1-078-2076) Cu_2O crystal structure without any CuO, suggesting no change in morphology or crystal structure, even after 22 days of visible light irradiation (laboratory light environment). However, for the sample washed with water, the CuO clearly formed a minor pattern. After 22 days, the XRD pattern of monoclinic ($C2/c$, JCPDS 41-0254) CuO was dominant, indicating almost complete oxidation of Cu_2O to CuO. The minor Cu_2O XRD signals from the oxidized samples were believed to be from the core of the Cu_2O cubes. In addition, the light yellow color of Cu_2O cubes changed to dark brown in water under laboratory light exposure, suggesting a change in material properties such as in oxidation state, as shown in the insets in Fig. 1.

To further understand the microstructures of the Cu_2O cubes and CuO nanoribbons, we obtained high-resolution TEM (HRTEM) images and selected area electron diffraction (SAED) patterns. Fig. 2A and B show the typical TEM images (more TEM images are available in the ESI,† Fig. S3) of the product obtained by keeping the as-synthesized Cu_2O cubes in ethanol and water with light exposure for 22 days, respectively. The microstructures of the product were found to be in good agreement with the SEM results. The shape of the Cu_2O cubes was unaffected when stored in ethanol for 22 days (Fig. 2A). Based on the TEM images, the cubes were 70–150 nm across the diagonal. The inset (left) in Fig. 2A shows the spot SAED pattern confirming the single crystal nature of Cu_2O cubes. A lattice spacing of 2.45 Å between the (111) planes of cubic Cu_2O was measured from the HRTEM as shown in the inset (right) in Fig. 2A.[27] However, Cu_2O cubes were found to be mostly reshaped to nanoribbons after 22 days in water with laboratory light exposure (Fig. 2B). It is important to note that no significant change in morphology was observed for the Cu_2O cubes stored in water under dark conditions. The length and width of these nanoribbons were found to range from 100 to 800 nm and 20 to 100 nm, respectively. The length of CuO nanoribbons was significantly

Published on 15 July 2014. Downloaded by Indian Institute of Technology Kharagpur on 18/12/2014 03:50:17.

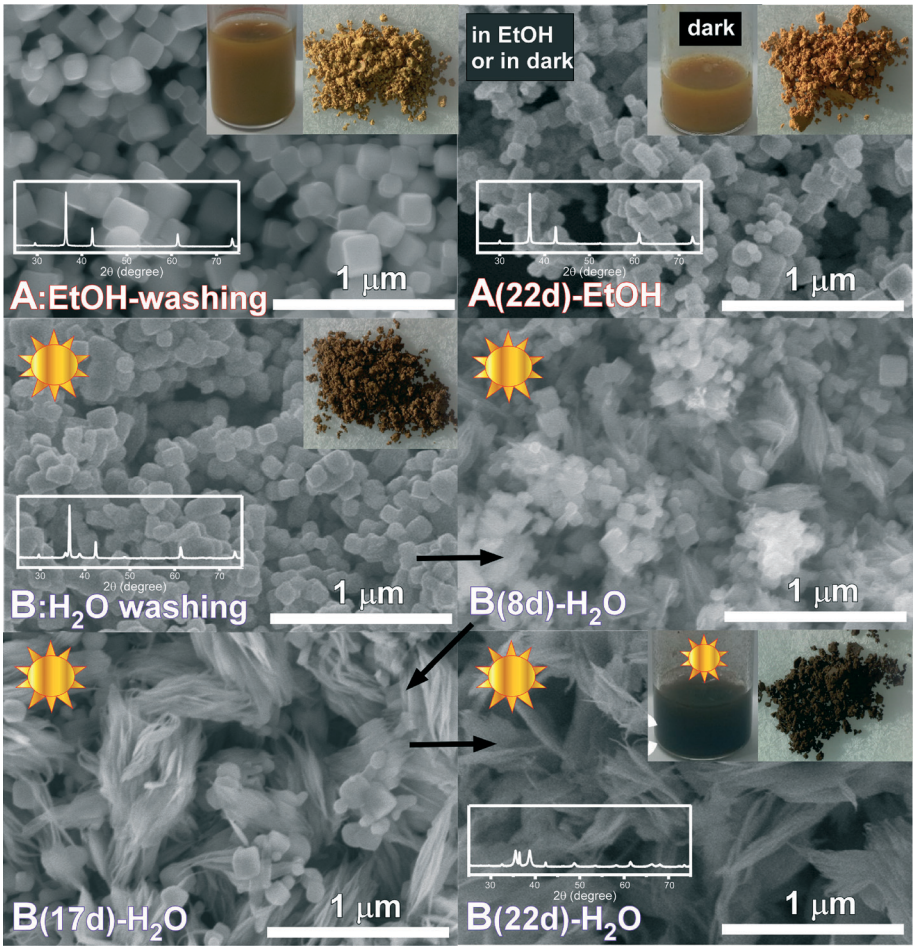

Fig. 1 SEM images of as-prepared Cu oxide samples washed with ethanol (A) and water (B) and of samples stored in ethanol (22 days) and water (8, 17, and 22 days). Insets show the optical microscope images and the XRD patterns of the corresponding samples.

longer than that of Cu_2O cubes. Furthermore, XRD and SAED analyses confirmed that these nanoribbons were phase changed to monoclinic CuO from the original cubic Cu_2O cubes (Fig. 1 inset and ESI,† Fig. S2). The spot SAED pattern (left inset, Fig. 2B) suggests a single crystal structure of nanoribbons with growth along [010].[28] The HRTEM image (right inset, Fig. 2B) shows a lattice spacing of 0.247 nm between the (002) planes of the CuO crystal with a monoclinic crystal structure. Fig. 2C and D clearly show CuO seeds and longer CuO ribbons on the edges of the Cu_2O cubes, suggesting the evolution of nanoribbons. These CuO ribbons were grown longer along [010] as the duration of light exposure increased.

We measured the UV-vis absorption spectra of the as-prepared Cu oxide powder and of the samples stored in ethanol and water for 22 days with light exposure (Fig. 3). The bandgap energy was estimated to be ~2.0 eV for the as-prepared sample and the Cu_2O cubes stored in ethanol. However, we measured a bandgap of 1.4 eV for the sample stored in water with light exposure, which is in good agreement with that of CuO.[33] The UV-vis absorption spectra support the change in oxidation state of Cu from +1 to +2 (from Cu_2O to CuO) when stored in water and under light illumination.

To further confirm the effects of light, we stored the Cu_2O cubes (dispersed in water) in the dark and under three different types of light (sunlight, fluorescent, and incandescent). Interestingly, under dark conditions, the cubes showed no critical change in powder color and morphology, even after 20 days (ESI,† Fig. S4). Conversely, the cubes changed color and morphology with time in the presence of light. The change in color from yellow to black was faster under incandescent irradiation than fluorescent light. In addition, the change in product morphology in response to radiation with different types of light was found to be dramatic, particularly in response to incandescent light (see also Fig. S5 in ESI†). It is obvious that the presence of water molecules (or moisture) and light accelerates the oxidation of Cu_2O (yellow) to CuO (black). These results confirmed the importance of visible light to the oxidation of Cu_2O to CuO.

To understand the recrystallization and oxidation mechanism (Cu_2O cubes to CuO nanoribbons), we employed an active species scavenger method. Ag^+ ions, isopropyl alcohol (IPA) and benzoquinone (BQ) were added to Cu_2O-dispersed water solution as scavengers for e^-, $^{\bullet}OH$ and $^{\bullet}O_2^-$, respectively.[56,57] Fig. 4 shows the XRD patterns of Cu_2O cubes dispersed in water with light exposure in the absence and

 This journal is © The Royal Society of Chemistry 2014

Published on 15 July 2014. Downloaded by Indian Institute of Technology Kharagpur on 18/12/2014 03:50:17.

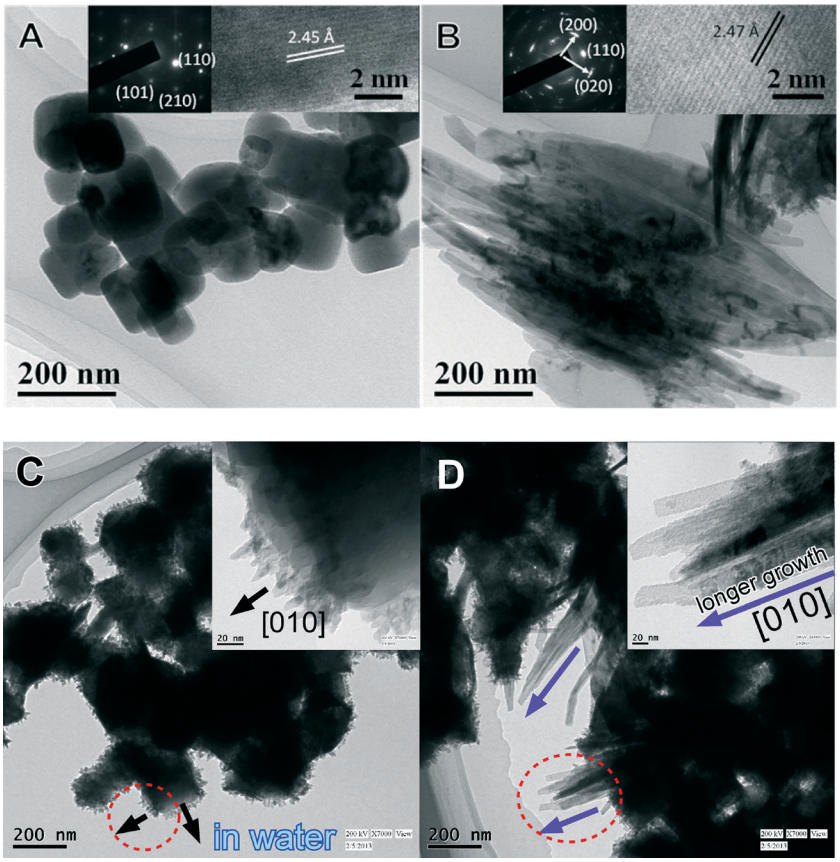

Fig. 2 TEM images of the Cu oxide samples stored in ethanol (A) and water (B) in the presence of laboratory light for 22 days. Insets show the corresponding HRTEM images and SAED patterns. TEM images (C and D) show CuO growth on the edges of Cu_2O cubes.

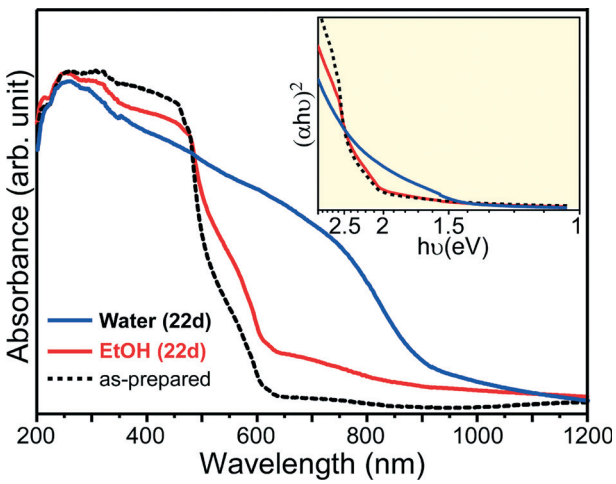

Fig. 3 Diffuse reflectance UV-visible absorption spectra of the as-prepared Cu oxide powder and of the samples stored in ethanol and water for 22 days with light exposure.

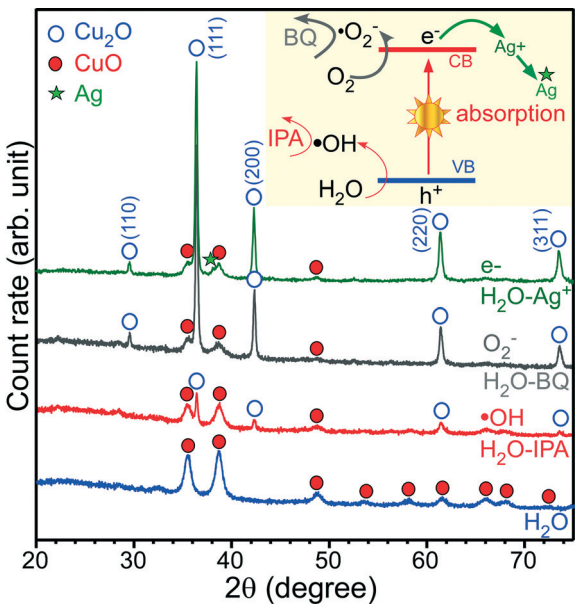

Fig. 4 XRD patterns of Cu_2O cubes dispersed in water with light exposure for 21 days in the absence and presence of scavengers (IPA, BQ and Ag^+). Inset shows the active species scavenging mechanism of the scavengers.

presence of scavengers (IPA, BQ and Ag^+). The XRD of Cu oxide in water with no scavenger showed only the patterns of CuO, indicating complete oxidation of Cu_2O cubes. However, in the presence of Ag^+ (an e^- acceptor) and BQ ($^{\bullet}O_2^-$ scavenger), the oxidation was dramatically suppressed, and no critical change in morphology was observed, even after 21 days. A metallic Ag XRD pattern was observed due to the reduction of Ag^+ ion in response to acceptance of the

Published on 15 July 2014. Downloaded by Indian Institute of Technology Kharagpur on 18/12/2014 03:50:17.

photogenerated electron. These findings affirm that the photogenerated electrons and $^{\bullet}O_2^-$ act as elemental species for the Cu_2O oxidation. When IPA ($^{\bullet}OH$ scavenger) was partially added into the water solution, the oxidation was suppressed, but to a lesser degree than when compared to the other two scavengers. When Cu_2O cubes were dispersed in IPA or ethanol (Fig. 1), no significant oxidation of Cu_2O was observed, indicating that $^{\bullet}OH$ radicals are also involved in the oxidation process.

A photoluminescence technique was applied to examine $^{\bullet}OH$ radical formation with Cu_2O cubes in water under light irradiation using terephthalic acid (TA).[56,57] TA reacts with $^{\bullet}OH$ to produce 2-hydroxyterephthalic acid, which emits broad luminescence at around 425 nm. Fig. 5 shows a strong emission peak at 425 nm, confirming $^{\bullet}OH$ radical formation and participation in Cu oxidation.

The photocatalytic dye degradation performance of Cu_2O cubes was examined by UV-vis absorption spectroscopy using methyl orange (MO) dye. This experiment was conducted under the assumption that when a dye (*i.e.* MO) is present in the solution and adsorbed on the surface of a Cu_2O cube, the active species ($^{\bullet}OH$ and $^{\bullet}O_2^-$) generated under light irradiation would participate in dye degradation, but not in the Cu_2O surface oxidation (ESI,† Fig. S6). In such a scenario, oxidation of Cu_2O was expected to be greatly suppressed, leading to insignificant changes in morphology. This was clearly observed in the SEM images (ESI,† inset in Fig. S6), confirming the role of active species in the oxidation process. Fig. 6 shows the UV-vis spectra and MO degradation performance. Furthermore, the dye degradation was significantly suppressed by active species scavengers as shown in Fig. 6. The $^{\bullet}OH$ radical scavenger effects were somewhat lower under UV light irradiation.

Fig. 7 summarizes the photocatalytic active species formation and recrystallization/oxidation schemes of Cu_2O cubes to CuO nanoribbons in water under light irradiation. Upon light irradiation, electrons and holes are created in the conduction and valence bands (CB and VB) of Cu_2O, respectively. The electrons in the CB are captured by the adsorbed molecular (or atomic) oxygen (an electron acceptor) on Cu_2O to form $^{\bullet}O_2^-$ (or $^{\bullet}O^-$), which acts as an active species for oxidation. These species and H^+ produce $^{\bullet}OH$ radicals. The VB hole reacts with OH^- or H_2O species to create $^{\bullet}OH$ radicals. As a result, the active species ($^{\bullet}O_2^-$ and $^{\bullet}OH$) on the Cu_2O surface proceed to an oxidation reaction as described below.

Under light irradiation:

Cu_2O + light → Cu_2O (e^-_{CB} + h^+_{VB})

Cu_2O (e^-_{CB}) + adsorbed O_2 (or adsorbed atomic O) → $^{\bullet}O_2^-$ (or $^{\bullet}O^-$)

$H_2O \rightarrow H^+ + OH^-$

$^{\bullet}O_2^-$ (or $^{\bullet}O^-$) + $H^+ \rightarrow {}^{\bullet}O_2H$ (or $^{\bullet}OH$)

OH^- + Cu_2O (h^+_{VB}) → $^{\bullet}OH$

H_2O + Cu_2O (h^+_{VB}) → H^+ + $^{\bullet}OH$

Cu_2O (h^+_{VB}) + $^{\bullet}O^- \rightarrow 2CuO$

$2Cu_2O$ (h^+_{VB}) + $^{\bullet}O_2{}^{2-} \rightarrow 4CuO$

$Cu_2O + 2{\cdot}OH \rightarrow 2CuO + H_2O$

The active species are captured in the presence of active species scavengers (Ag^+, BQ and IPA) and therefore cannot participate in the oxidation reaction and [010]-directed CuO nanoribbon formation. In addition, when adsorbed dye such as MO is present on the Cu_2O surface, the active species participate in the dye degradation without reacting with the Cu_2O surface. Consequently, no CuO is formed, as was observed in the present study.

It is important to discuss the thermal Cu and Cu_2O oxidation ($2Cu_2O + O_2 \rightarrow 4CuO$) in the presence of oxygen at high temperature (*i.e.* gas/solid interface oxidation reaction) to understand the recrystallization and oxidation mechanism.[32] This oxidation is known to be due to the faster outward diffusion of copper relative to the inward diffusion of oxygen.[29,34,36] Therefore, Cu atoms diffuse through the Cu_2O layer and react with ambient oxygen, resulting in the formation of CuO seed on the Cu_2O surface and the subsequent growth of CuO with a nanowire or nanoribbon morphology.[32–39] The outward diffusion of copper atoms in Cu_2O was considered the rate-determining step for the nanowire/nanoribbon growth.[39] However, in a hydrothermal (or solvothermal) method, $Cu(OH)_2$ nanosheets (wires and ribbons) were reportedly produced in the presence of basic OH^- solution under dark conditions, and those nanosheets were thermally dehydrated into CuO as follows:[26,34,36] $Cu_2O + 2OH^- \rightarrow 2CuO + H_2O + 2e^-$, $Cu(OH)_2 \rightarrow CuO + H_2O$, where CuO nanobelts (or nanorods) were grown along the [010] direction by the thermal dehydration of $Cu(OH)_2$ nanowires.[30,31] Based on the reported mechanism and results of the present study, we propose a possible growth mechanism of CuO *via* the room temperature light-induced oxidation process described herein. Fig. 8 shows the projection of cubic Cu_2O (bottom left) and monoclinic CuO structures (top) along the [010] direction, where the [010] growth direction of CuO is more clearly displayed. As the (010) plane is least stable in monoclinic CuO,[29] growth primarily occurs on the plane forming two-dimensional structures, as observed in the present study. Fig. 8 (bottom right),

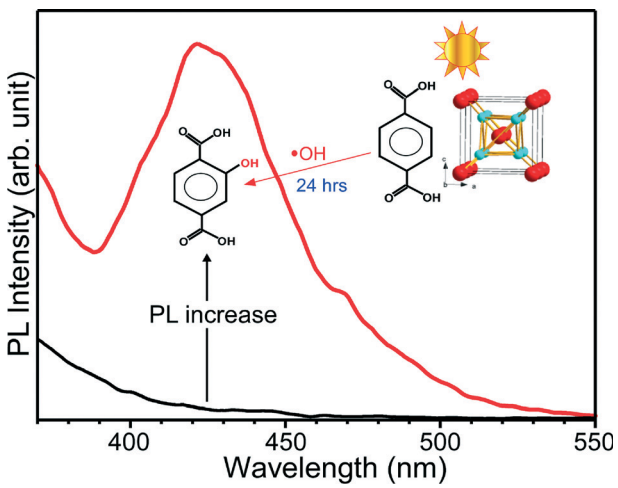

Fig. 5 Photoluminescence spectra of terephthalic acid solution with Cu_2O cubes in water before and after light irradiation.

 This journal is © The Royal Society of Chemistry 2014

Published on 15 July 2014. Downloaded by Indian Institute of Technology Kharagpur on 18/12/2014 03:50:17.

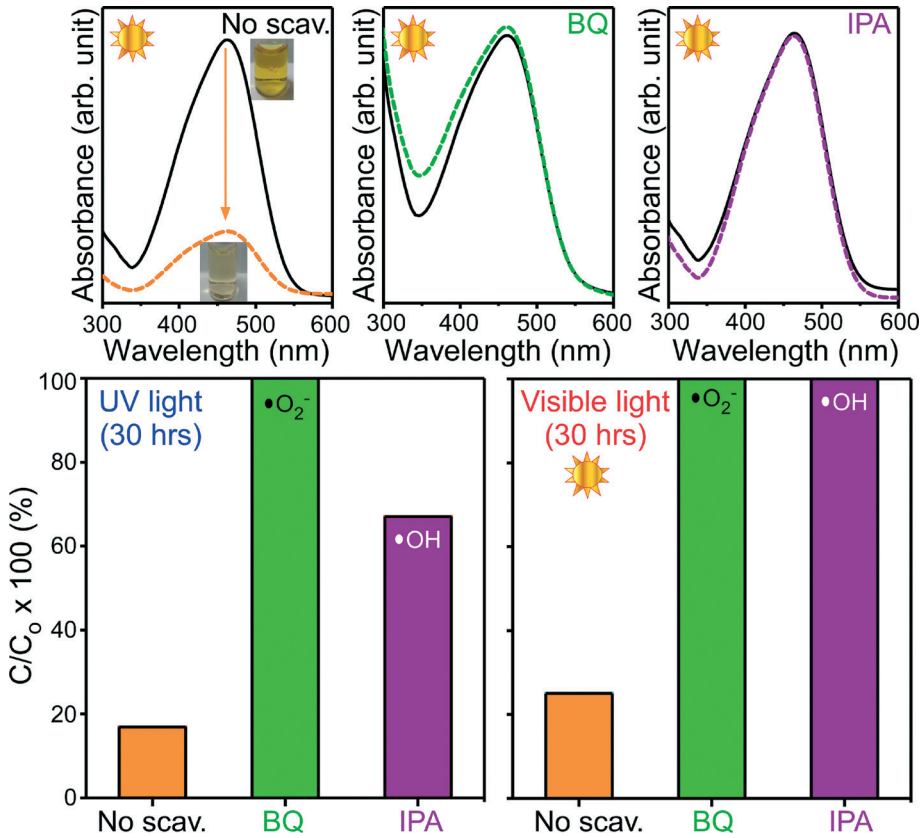

Fig. 6 Photocatalytic degradation of MO (10 mg L^{-1}) with Cu_2O cubes in the absence and presence of scavengers (BQ and IPA) with light exposure.

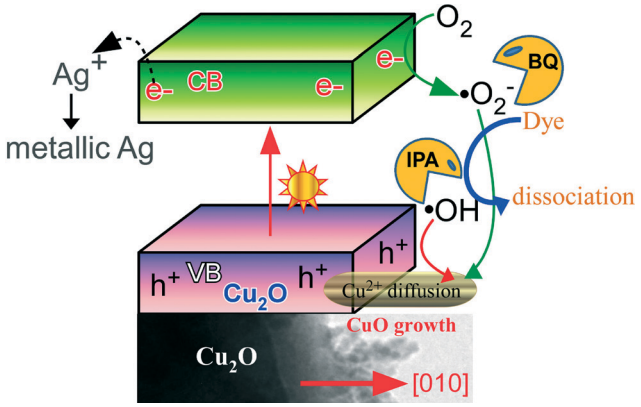

Fig. 7 Photocatalytic active species formation and recrystallization/oxidation scheme of Cu_2O cubes to CuO nanoribbons in water under visible light irradiation.

SEM (Fig. 1) and TEM (Fig. 2) images clearly show the quasi one-dimensional outward CuO growth on the edge of Cu_2O cubes. This can be attributed to the outward diffusion of Cu ions during recrystallization by room temperature light-induced liquid/solid (water/Cu_2O) interface oxidation reaction. CuO initially nucleates the surface of the Cu_2O cube and subsequently evolves to longer nanoribbons as the Cu ion diffuses outward and active species ($^{\bullet}O_2^-$ and $^{\bullet}OH$) are generated. It appears that inward diffusion of the active species is much slower than the outward Cu diffusion. Such outward diffusion of Cu cations is likely driven by surface CuO/Cu_2O interfacial stress.[32] This interfacial stress, which arises upon oxidation of the Cu_2O cube surface to CuO, leads to outward growth of the CuO ribbon-like structure from the Cu_2O cube surface in a process similar to capillary action. As a result, the quasi one-dimensional ribbon structure of CuO grows along its unstable {010} facets.[30] The growth of ribbons proceeds with a continuous supply of Cu cations from Cu_2O cubes until it is fully consumed. Overall, the light-induced oxidation of Cu_2O to CuO could be a simple model for understanding the oxidation mechanism in both gas and light-off/on liquid phases, as well as gas/solid and liquid/solid interfacial oxidation reactions.

For potential application of Cu oxides, we further demonstrated the catalytic performance of Cu_2O cubes and CuO nanoribbons for CO oxidation. Fig. 9 shows CO conversion (%) *versus* reaction temperature (°C) for cubes and nanoribbons stored in ethanol and water for 22 days, respectively. In the 1st test runs for the cubes and nanoribbons, $T_{10\%}$ (the temperature at which 10% CO conversion to CO_2 occurs) was found to be 278 °C and 245 °C, respectively. In the 2nd test runs, the CO_2 signal for nanoribbons started to appear at 155 °C, and $T_{10\%}$ occurred at 191 °C. The catalytic activity was improved by 54 °C relative to the 1st run. In the 2nd test run for the cubes, $T_{10\%}$ was found at 333 °C, indicating that the catalytic

Published on 15 July 2014. Downloaded by Indian Institute of Technology Kharagpur on 18/12/2014 03:50:17.

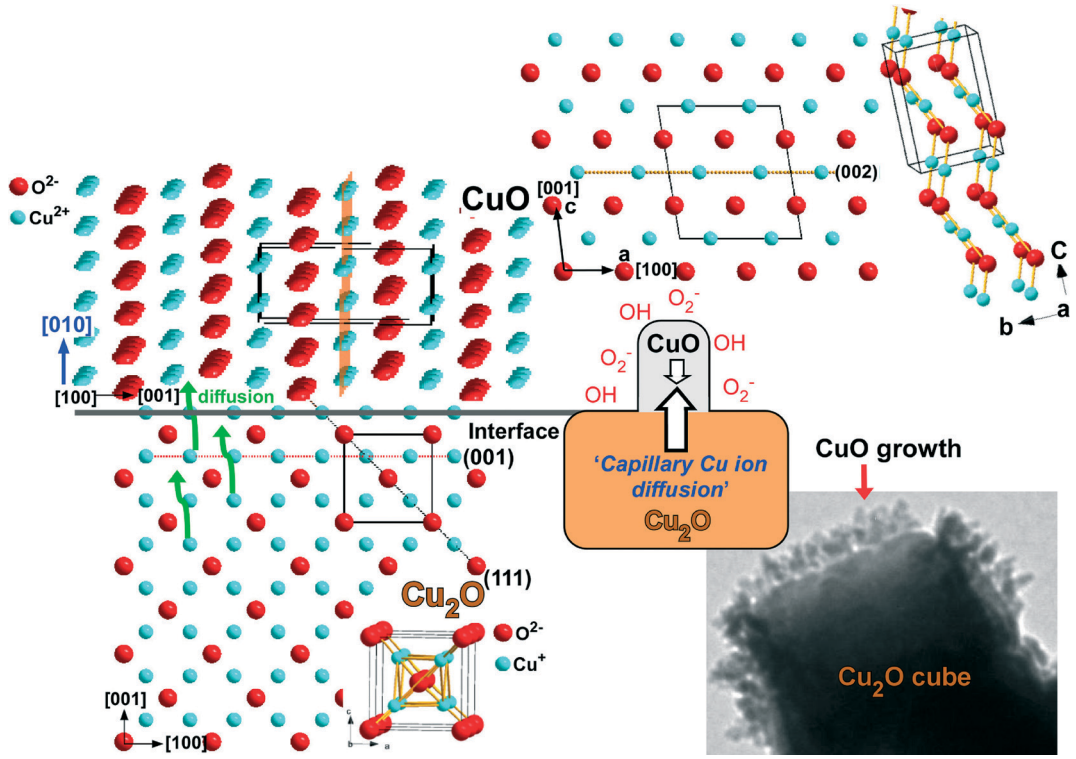

Fig. 8 Projection of Cu_2O (bottom left) and CuO structures (top three) along the [010] direction. The [010] growth direction is shown on the surface of Cu_2O. The TEM image (bottom right) shows CuO seed on the surface of the Cu_2O cube.

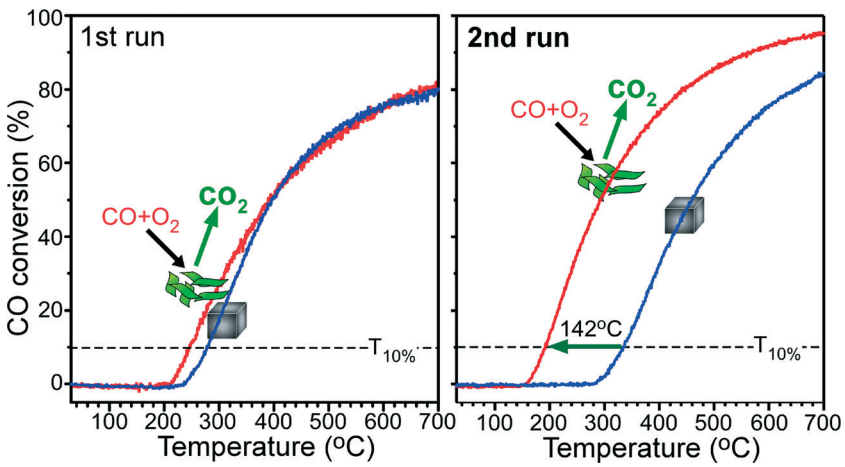

Fig. 9 1st and 2nd CO oxidation test runs of Cu oxide samples stored in ethanol (22 days, Cu_2O with cube morphology) and water (22 days, CuO with nanoribbon morphology).

activity for Cu_2O (stored in ethanol for 22 days) was decreased by 55 °C when compared to the 1st run. This is likely due to the change in the crystal facet after the 1st CO oxidation. The $T_{10\%}$ of nanoribbons was significantly lower (142 °C) than that of the cubes. The higher CO oxidation activity for CuO nanoribbons was due to its high surface area and surface lattice oxygen. The BET surface area of the as-prepared Cu_2O cubes was measured to be 9.3 $m^2\ g^{-1}$. The surface area was significantly increased (2.6×) to 24.3 $m^2\ g^{-1}$ upon recrystallization to CuO nanoribbons from Cu_2O cubes. Carbon dioxide (CO_2) is known to be formed *via* the following mechanism: $CO + [O]^*\text{–}Cu \rightarrow CO_2 + [O]_{vac}\text{–}M$, where $[O]^*\text{–}Cu$ is the active surface oxygen formed by $Cu + 1/2O_2 \rightarrow [O]_{vac}\text{–}M$ and $[O]_{vac}\text{–}M$ is a surface oxygen vacancy.[52,54,55] The richness of $[O]^*\text{–}Cu$ over CuO nanoribbons may determine the higher CO oxidation activity. Kim *et al.* reported that when CuO thorns were grown on the surface of Cu_2O nanocrystals, the CO oxidation activity was enhanced.[53] Cu_2O has also been reported to be more active than CuO.[49,52] However, other factors such as morphology likely influence the CO oxidation

 This journal is © The Royal Society of Chemistry 2014

Published on 15 July 2014. Downloaded by Indian Institute of Technology Kharagpur on 18/12/2014 03:50:17.

activity.[54,55] As shown in the SEM images of cubes and nanoribbons after CO oxidation (ESI,† Fig. S7), the morphologies were slightly changed. The activation energies (E_a, kJ mol^{-1}) were calculated from the Arrhenius plots (ESI,† Fig. S8) in the kinetic region ($T_{10\%}$ = 10–15%). The reaction rate (v) was calculated using the equation v = (molar CO flow rate, mol s^{-1}) × (CO conversion fraction)/(catalyst weight, g_{cat}).[58,59] In the 1st test runs, the activation energies (kJ mol^{-1}) were measured to be 68.0 and 51.4 kJ mol^{-1} for the cubes and nanoribbons, respectively. In the 2nd run, the values were 75.5 and 57.6 kJ mol^{-1}, respectively, which is consistent with the literature.[52]

4. Conclusions

In this study, we demonstrated the light-induced oxidation and recrystallization of Cu_2O cubes to [010] growth-directed CuO nanoribbons in water at room temperature for the first time. Upon light irradiation, electrons and holes are generated in the Cu_2O cubes, resulting in creation of active species ($^{\bullet}O_2^-$ and $^{\bullet}OH$) in water that subsequently participate in oxidation reactions on the Cu_2O surface. The role of active species was confirmed by introducing an electron acceptor (*e.g.*, Ag^+ ion), active species scavengers (IPA and BQ) and MO dye, each of which suppressed Cu_2O oxidation. The growth of a quasi one-dimensional CuO ribbon along its unstable {010} facets was attributed to the outward diffusion of Cu cations, interfacial stress at CuO/Cu_2O and active species generated on the surface. CO oxidation over the CuO nanoribbon started to appear at 155 °C with an activation energy of 57.6 kJ mol^{-1}. The CO oxidation activity of the nanoribbons was superior to that of the cubes. Our unique visible light-induced recrystallization of Cu_2O to CuO in water provides new insight into understanding surface stability, oxidation mechanisms and photocatalytic reactions and tailoring nanostructures by varying light. This work also provides a new strategy for the development of energy- and environment-related Cu oxide nanomaterials.

Acknowledgements

This work was financially supported by the National Research Foundation of Korea (NRF) grant funded by the Korea government (MEST) (NRF-2011-0025386 and NRF-2012R1A1A4A01005645) and the Department of Science and Technology, New Delhi, through the grant Indo-Korea/P-02.

References

1 M. Yin, C.-K. Wu, Y. Lou, C. Burda, J. T. Koberstein, Y. Zhu and S. O'Brien, *J. Am. Chem. Soc.*, 2005, **127**, 9506.
2 J. Y. Kim, J. A. Rodriguez, J. C. Hanson, A. I. Frenkel and P. L. Lee, *J. Am. Chem. Soc.*, 2003, **125**, 10684.
3 S. Deng, V. Tjoa, H. M. Fan, H. R. Tan, D. C. Sayle, M. Olivo, S. Mhaisalkar, J. Wei and C. H. Sow, *J. Am. Chem. Soc.*, 2012, **134**, 4905.
4 W.-C. Huang, L.-M. Lyu, Y.-C. Yang and M. H. Huang, *J. Am. Chem. Soc.*, 2012, **134**, 1261.
5 A. Radi, D. Pradhan, Y. Sohn and K. T. Leung, *ACS Nano*, 2010, **4**, 1553.
6 Y. Bai, T. Yang, Q. Gu, G. Cheng and R. Zheng, *Powder Technol.*, 2012, **227**, 35.
7 Q. Hua, K. Chen, S. Chang, Y. Ma and W. Huang, *J. Phys. Chem. C*, 2011, **115**, 20618.
8 J. C. Park, J. Kim, H. Kwon and H. Song, *Adv. Mater.*, 2009, **21**, 803.
9 Y. Zhang, B. Deng, T. Zhang, D. Gao and A.-W. Xu, *J. Phys. Chem. C*, 2010, **114**, 5073.
10 Z. Zheng, B. Huang, Z. Wang, M. Guo, X. Qin, X. Zhang, P. Wang and Y. Dai, *J. Phys. Chem. C*, 2009, **113**, 14448.
11 K. X. Yao, X. M. Yin, T. H. Wang and H. C. Zeng, *J. Am. Chem. Soc.*, 2010, **132**, 6131.
12 X. Lan, J. Zhang, H. Gao and T. Wang, *CrystEngComm*, 2011, **13**, 633.
13 L. I. Hung, C.-K. Tsung, W. Huang and P. Yang, *Adv. Mater.*, 2010, **22**, 1910.
14 B. Luo, X. Li, X. Li, L. Xue, S. Li and X. Li, *CrystEngComm*, 2013, **15**, 5654.
15 C. Qiu, Y. Bao, N. L. Netzer and C. Jiang, *J. Mater. Chem. A*, 2013, **1**, 8790.
16 H. Li, Y. Ni, Y. Cai, L. Zhang, J. Zhou, J. Hong and X. Wei, *J. Mater. Chem.*, 2009, **19**, 594.
17 S. Sun, X. Zhang, X. Song, S. Liang, L. Wang and Z. Yang, *CrystEngComm*, 2012, **14**, 3545.
18 G. Prabhakaran and R. Murugan, *CrystEngComm*, 2012, **14**, 8338.
19 A.-L. Daltin, A. Addad, P. Baudart and J.-P. Chopart, *CrystEngComm*, 2011, **13**, 3373.
20 L. Hu, Y. Huang, F. Zhang and Q. Chen, *Nanoscale*, 2013, **5**, 4186.
21 B. Heng, C. Qing, D. Sun, B. Wang, H. Wang and Y. Tang, *RSC Adv.*, 2013, **3**, 15719.
22 K. Chen and D. Xue, *Appl. Sci. Converg. Technol.*, 2014, **23**, 14.
23 K. Chen and D. Xue, *CrystEngComm*, 2013, **15**, 1739.
24 K. Chen and D. Xue, *Phys. Chem. Chem. Phys.*, 2013, **15**, 19708.
25 K. Chen and D. Xue, *J. Phys. Chem. C*, 2013, **117**, 22576.
26 Y. Sun, L. Ma, B. Zhou and P. Gao, *Int. J. Hydrogen Energy*, 2012, **37**, 2336.
27 W. Wang, G. Wang, X. Wang, Y. Wang, Y. Zhan and Y. Liu, *et al.*, *Adv. Mater.*, 2002, **14**, 67.
28 T.-Y. Dong, C. N. Chen, H.-Y. Cheng, C. P. Chen and N.-Y. Jheng, *Inorg. Chim. Acta*, 2011, **367**, 158.
29 Z. Zhang, H. Sun, X. Shao, D. Li, H. Yu and M. Han, *Adv. Mater.*, 2005, **17**, 42.
30 G. H. Du and G. V. Tendeloo, *Chem. Phys. Lett.*, 2004, **393**, 64.
31 H. Chen, D.-W. Shin, J. H. Lee, S.-M. Park, K.-W. Kwon and J.-B. Yoo, *J. Nanosci. Nanotechnol.*, 2010, **10**, 5121.
32 L. Yuan, Y. Wang, R. Mema and G. Zhou, *Acta Mater.*, 2011, **59**, 2491.
33 A. Chen, H. Long, X. Li, Y. Li, G. Yang and P. Lu, *Vacuum*, 2009, **83**, 927.

Published on 15 July 2014. Downloaded by Indian Institute of Technology Kharagpur on 18/12/2014 03:50:17.

34 K. Chen, S. Song and D. Xue, *CrystEngComm*, 2013, **15**, 144.
35 A. Li, H. Song, J. Zhou, X. Chen and S. Liu, *CrystEngComm*, 2013, **15**, 8559.
36 S. L. Shinde and K. K. Nanda, *RSC Adv.*, 2012, **2**, 3647.
37 R. Mema, L. Yuan, Q. Du, Y. Wang and G. Zhou, *Chem. Phys. Lett.*, 2011, **512**, 87.
38 Q. Zhang, K. Zhang, D. Xu, G. Yang, H. Huang, F. Nie, C. Liu and S. Yang, *Prog. Mater. Sci.*, 2014, **60**, 208.
39 S.-K. Lee and W.-H. Tuan, *Mater. Lett.*, 2014, **117**, 101.
40 Y. Song, E. E. Doomes, J. Prindle, R. Tittsworth, J. Hormes and C. S. S. R. Kumar, *J. Phys. Chem. B*, 2005, **109**, 9330.
41 Y. Song, R. Li, Q. Sun and P. Jin, *Chem. Eng. J.*, 2011, **168**, 477.
42 Q. Yu, H. Huang, R. Chen, P. Wang, H. Yang, M. Gao, X. Peng and Z. Ye, *Nanoscale*, 2012, **4**, 2613.
43 S. Sun, X. Song, Y. Sun, D. Deng and Z. Yang, *Catal. Sci. Technol.*, 2012, **2**, 925.
44 X. Meng, G. Tian, Y. Chen, Y. Qu, J. Zhou, K. Pan, W. Zhou, G. Zhang and H. Fu, *RSC Adv.*, 2012, **2**, 2875.
45 M. Hara, T. Kondo, M. Komoda, S. Ikeda, K. Shinohara, A. Tanaka, J. N. Kondo and K. Domen, *Chem. Commun.*, 1998, 357.
46 S. Kakuta and T. Abe, *Electrochem. Solid-State Lett.*, 2009, **12**, P1.
47 C.-C. Hu, J.-N. Nian and H. Teng, *Sol. Energy Mater. Sol. Cells*, 2008, **92**, 1071.
48 B. White, M. Yin, A. Hall, D. Le, S. Stolbov, T. Rahman, N. Turro and S. O'Brien, *Nano Lett.*, 2006, **6**, 2095.
49 Y. Feng and X. Zheng, *Nano Lett.*, 2010, **10**, 4762.
50 Q. Hua, T. Cao, H. Bao, Z. Jiang and W. Huang, *ChemSusChem*, 2013, **6**, 1966.
51 M. Leng, M. Liu, Y. Zhang, Z. Wang, C. Yu, X. Yang, H. Zhang and C. Wang, *J. Am. Chem. Soc.*, 2010, **132**, 17084.
52 T.-J. Huang and D.-H. Tsai, *Catal. Lett.*, 2003, **87**, 173.
53 J. Kim, Y. Kwon and H. Lee, *J. Mater. Chem. A*, 2013, **1**, 14183.
54 D. A. Svintsitskiy, A. P. Chupakhin, E. M. Slavinskaya, O. A. Stonkus, A. I. Stadnichenko, S. V. Koscheev and A. I. Boronin, *J. Mol. Catal. A: Chem.*, 2013, **368–369**, 95.
55 D. A. Svintsitskiy, T. Yu. Kardash, O. A. Stonkus, E. M. Slavinskaya, A. I. Stadnichenko, S. V. Koscheev, A. P. Chupakhin and A. I. Boronin, *J. Phys. Chem. C*, 2013, **117**, 14588.
56 W. Kim, D. Pradhan, B. K. Min and Y. Sohn, *Appl. Catal., B*, 2014, **147**, 711.
57 Y. Park, Y. Na, D. Pradhan, B.-K. Min and Y. Sohn, *CrystEngComm*, 2014, **16**, 3155.
58 S. W. Lee, S. K. Park, B. K. Min, J. G. Kang and Y. Sohn, *Appl. Surf. Sci.*, 2014, **307**, 736.
59 Y. Park, S. K. Kim and D. Pradhan, *Chem. Eng. J.*, 2014, **250**, 25.

 This journal is © The Royal Society of Chemistry 2014